*Int. J. Solids Structures* Vol. 25, No. 7, pp. 729–749, 1989
Printed in Great Britain.

0020–7683/89 $3.00 + .00


# INTERACTIVE BUCKLING IN THIN-WALLED BEAMS—II. APPLICATIONS

P. GOLTERMANN† and H. MØLLMANN
Department of Structural Engineering, Technical University of Denmark, 2800 Lyngby, Denmark

(*Received* 29 *April* 1987; *in revised form* 21 *October* 1988)

**Abstract**—Mode interaction between local and global buckling modes is studied for two types of thin-walled beam structures, using a method of analysis presented in Part I of the author's paper [Møllmann and Goltermann (1989). *Int. J. Solids Structures* **25**, 715–728]. This method involves a combination of the finite strip method and Koiter's asymptotic theory of stability. It appears that the interaction essentially involves three buckling modes (one global and two local modes), and that the inclusion of additional nearly simultaneous local buckling modes in the analysis does not alter the results perceptibly (in the case of local imperfections). In both examples, substantial reductions of load-carrying capacity due to mode interaction and imperfection sensitivity (up to about 50%) are observed. Some of the 2nd order fields and 4-index coefficients exhibit a marked dependence on the value of the load factor at which they are evaluated. For both structures, the load-carrying capacities have been determined for different values of the ratio between global and local critical loads. When this ratio is greater than one (i.e. when the local critical load is smaller than the global), the load carrying capacity will exceed the local critical load if the imperfections are sufficiently small.

## NOTATION

| | |
|---|---|
| $A$ | cross-sectional area of beam |
| $E$ | modulus of elasticity |
| $L$ | length of beam or column |
| $L_{wave}^{(i)}$ | half wavelength of mode $i$ |
| $M$ | characteristic bending moment |
| $N$ | characteristic compression load |
| $a_{,jk}$ | 3-index coefficient in the nonlinear eqns (15) in Part I |
| $a_{,jkm}$ | 4-index coefficient |
| $b$ | width of square cross-section |
| $f_i$ | amplitude of mode $i$ |
| $f_i^*$ | imperfection of same form as mode $i$ |
| $f_{global}, f_{local}$ | amplitude of global and local mode |
| $f_{global}^*, f_{local}^*$ | global and local imperfection |
| $h$ | height of I-cross-section |
| $t$ | thickness of plates |
| $\mathbf{u}_i$ | mode $i$ |
| $\mathbf{u}_{,j}$ | 2nd order field |
| $\lambda$ | load parameter |
| $\lambda_i^{(i)}$ | critical load corresponding to mode $i$ |
| $\lambda^{(global)}, \lambda^{(local)}$ | global and local critical load |
| $\lambda_{max}$ | load-carrying capacity |
| $\lambda_p$ | the $\lambda$-value used in the computation of $\mathbf{u}_{,j}$ |

## 1. INTRODUCTION

The present paper is the second part of an investigation dealing with mode interaction in thin-walled beams (Part I: Møllmann and Goltermann, 1989). Mode interaction in these structures occurs when the critical loads of overall and local buckling are nearly the same, and it usually involves the interaction between one overall, long-wave buckling mode, and one or more local, short-wave buckling modes. The method used by us to study these interaction phenomena is based on the nonlinear theory of elasticity and the general theory of stability. The background of the method and its relation to existing work in this field is discussed in the introduction to our first paper (see Part I, Section 1). The main features of

† Also at Rambøll & Hannemann, Consulting Engineers, Teknikerbyen 38, 2830 Virum, Denmark.

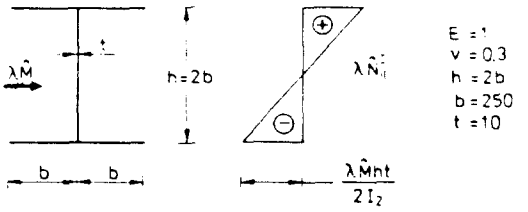


Fig. 1. Cross-section and stress distribution in the I-beam.

the method may be summarized as follows: the thin-walled beam is composed of plane, rectangular plate segments interconnected along longitudinal edges. A nonlinear finite displacement plate theory is used to describe the behaviour of the segments. The complete, nonlinear expressions for the middle surface strains are used, but the formulae for the changes of curvature are linearized. Assuming an elastic material and "dead" loading, an expression for the total potential energy of the structure is derived (in this derivation, it is assumed that the displacements of the pre-buckling equilibrium state may be neglected). Koiter's asymptotic theory of stability is used to study the post-buckling behaviour and the imperfection sensitivity, the buckling modes and the 2nd order displacement fields being determined by the finite strip method. A detailed derivation of the method is given in Part I. An attractive feature of this method is that it is capable of describing the complete range of behaviour of the thin-walled beam from local to global stability.

The present paper describes the application of the theory to two examples of commonly used thin-walled beam structures. The first example is concerned with a beam of doubly symmetrical I-section and loaded by equal and opposite bending moments at the ends (overall buckling therefore takes place as lateral buckling). The second example is concerned with a column of square box-section and loaded by axial compressive forces at the ends (in this case overall buckling takes place as flexural column buckling). The beams are in both cases simply supported at the ends. It will appear from the following that significant mode interaction and imperfection sensitivity occur in both examples.

## 2. SYMMETRICAL BENDING OF I-BEAM

We wish to investigate the mode interaction and imperfection-sensitivity of an I-beam with a doubly-symmetrical cross-section as shown in Fig. 1. The beam is simply supported and loaded by equal and opposite bending moments ($\lambda\hat{M}$) at the ends which result in a constant bending moment throughout the beam, and a stress distribution in the cross-section as shown in Fig. 1. We choose the characteristic bending moment ($\hat{M}$) as

$$\hat{M} = 1$$

thereby making

$$M = \lambda\hat{M} = \lambda.$$

We may now calculate the three lowest critical loads ($\lambda_c$) and their associated modes at certain half wavelengths ($L_{wave}$) by means of the finite strip method as explained in Part I, Section 4. The values of $\lambda_c$ depend on $L_{wave}$ as shown in Fig. 2, and the corresponding modes at some representative half wavelengths are shown in Fig. 3.

In order to investigate the interaction, we choose one global and two of the local modes as buckling modes (1st order fields) in our interaction analysis (see Section 3 in Part I). The global mode ($\mathbf{u}_1$ in Fig. 4) has a half wavelength $L^{(1)}_{wave}$ equal to the total length of the beam $L$, whereas the half wavelength of the two local modes ($\mathbf{u}_2$ and $\mathbf{u}_3$ in Fig. 4) is determined by the local minimum on the lowest $\lambda_c$-curve in Fig. 2. This minimum corresponds to $L_{wave} = 1.3h$, which is chosen as half wavelength of both the local modes, thereby limiting the total length of the beam to a multiple of $L^{(2)}_{wave} = L^{(3)}_{wave} = 1.3h$.

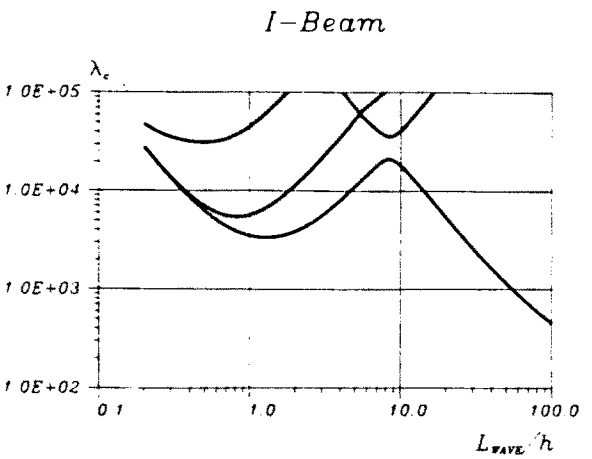


Fig. 2. Critical load versus half wavelength.

We wish to study the interaction at different values of $\lambda_c^{(\text{global})}/\lambda_c^{(\text{local})} = \lambda_c^{(1)}/\lambda_c^{(2)}$. To do this we investigate beams with $L/h$ equal to 13.0, 15.6, 18.2, 20.8, 26.0 and 36.4, corresponding to $(\lambda_c^{(\text{global})}/\lambda_c^{(\text{local})})$-values of 3.57, 2.57, 1.93, 1.51, 1.01 and 0.57. The three $\lambda_c$-values and their corresponding modes ($\mathbf{u}_i$) are calculated at each beam length. The modes are normalized using (9a) in Part I and further calculations show that the 3-index coefficients generally vanish, i.e.

$$a_{ijk} = 0, \quad i, j, k \in \{1, 2, 3\} \tag{1}$$

except that

$$a_{123} \neq 0$$

as shown in Table 1, for the case of $L/h = 13.0$.

Since $a_{123} \neq 0$, it is possible to obtain an estimate of the imperfection-sensitivity based on the 1st order fields only, provided that we use a 3-mode analysis (a 2-mode analysis will not be sufficiently accurate without a calculation of the 2nd order fields). However, we shall generally include the 2nd order fields in our analysis, and we shall calculate these fields at various $\lambda$-values ($\lambda_p$). This will enable us to include the 4th degree terms in the energy expression and to investigate load-carrying capacities above the local critical load, as explained in the following.

The fact that $a_{123}$ is the only 3-index coefficient that is different from zero means, according to (32a) in Part I, that the mixed local-global 2nd order fields $\mathbf{u}_{12}$ and $\mathbf{u}_{13}$ will depend significantly on the $\lambda$-value at which they are calculated ($\lambda_p$), and it also means that the dominant part of $\mathbf{u}_{12}$ will consist of local modes of the same type as $\mathbf{u}_3$, and $\mathbf{u}_{13}$ of local modes of the same type as $\mathbf{u}_2$. The 2nd order fields $\mathbf{u}_{11}$, $\mathbf{u}_{22}$, $\mathbf{u}_{33}$ and $\mathbf{u}_{23}$ will only show a slight $\lambda_p$-dependence, which means that only the mixed 4-index coefficients $a_{1122}$ and $a_{1133}$ will be significantly $\lambda_p$-dependent, whereas the coefficients $a_{1111}$, $a_{2222}$, $a_{2233}$ and $a_{3333}$ will only depend slightly on $\lambda_p$. The 2nd order fields are calculated by the finite strip method as explained in Part I, Section 4, and are described by Fourier-expansions in the longitudinal direction. In order to illustrate their shape, we let the computer plot the shape in different cross-sections as shown in Fig. 5. The deflections perpendicular to the beam-axis ($v, w$) are shown in the bottom row of the figure and are easily visualized. However, it should be noted that the displacement ($u$) and the stress (sigma 11) in the longitudinal direction are plotted along lines inclined at 45°, positive upwards to the right.

We can now calculate the 4-index coefficients $a_{ijkm}$. When we insert the 1st and 2nd order fields directly into formula (29a) in Part I, the convergence is found to be very slow, but when we use a Fourier-expansion of the contribution from the 1st order fields (as explained in Part I, Section 4) we obtain a much improved accuracy.

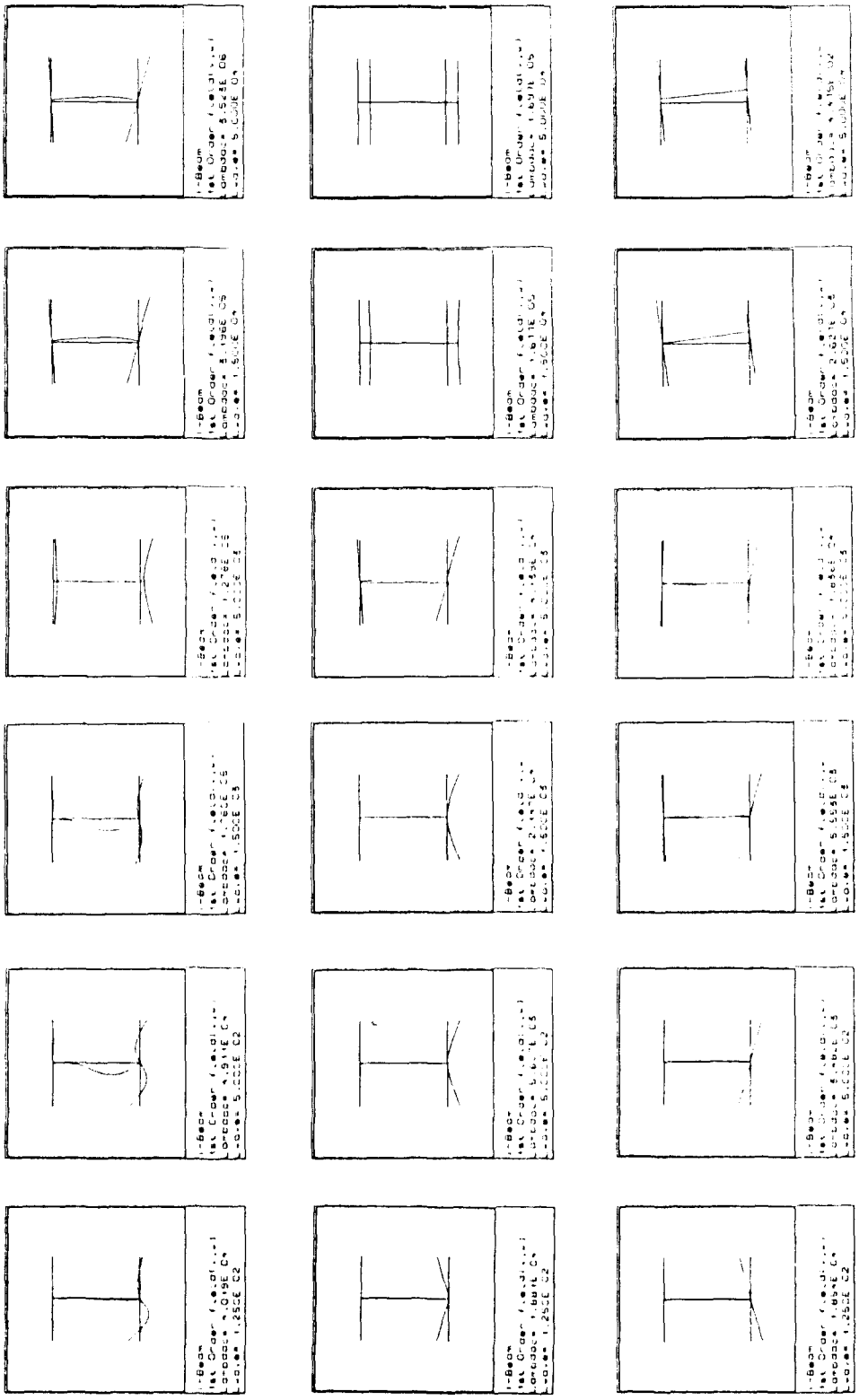

Fig. 3. Modes of different half wavelengths ($L_{max}$, $h = 1, 2, 1, 3, 10, 30$, and 100).

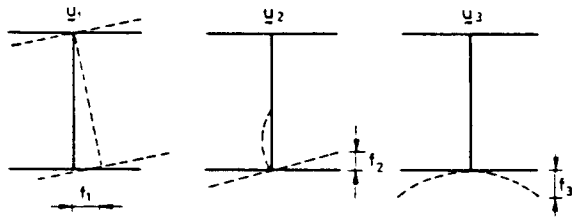


Fig. 4. Definition of amplitudes of the buckling modes.

In the case of $a_{1111}$, the convergence of the two methods is shown in Fig. 6, where $a_{1111}$ is compared with the results from beam-theory using Vlasov's assumptions (see Møllmann, 1982; Pedersen, 1982; and Goltermann, 1985).

In both our examples we use eight strips for each side of the cross-section (i.e. flange or web), and in our Fourier-expansion of the 2nd order fields we usually include 35 terms. This was found to provide adequate accuracy in all cases, although it would occasionally have been sufficient to use a smaller number of strips and Fourier terms.

We have now calculated the critical loads, the 1st and 2nd order fields, and the 3- and 4-index coefficients, see Table 1 for $L/h = 13.0$. This enables us to study the interaction and imperfection sensitivity by solving the non-linear equilibrium equations (15) in Part I. The solutions of these equations determine a system of equilibrium paths of the type shown in Fig. 7 for the case of two modes.

Consider the perfect structure under increasing load, starting from the unloaded state. For small values of the load, the equilibrium path coincides with the $\lambda$-axis (the prebuckling path). However, when the load reaches the smallest critical load $\lambda_c$, the solution bifurcates (point A in Fig. 7). This 1-mode bifurcation will often be stable-symmetric and we may in this case increase the load above $\lambda_c$, due to the post-critical stiffness, until a second bifurcation is reached. This unstable bifurcation (point B in Fig. 7) determines the ultimate load-carrying capacity $\lambda_{max}$ and appears because of the interaction. In the case of the imperfect structure, the $\lambda_{max}$-value will be determined by a load maximum except in the situation where the imperfection corresponds to the mode of the lowest critical load, where $\lambda_{max}$ will be determined by a bifurcation, provided that this mode corresponds to a stable-symmetric bifurcation (as will be the case for the local mode). The solution of the equations and the determination of the load-carrying capacity $\lambda_{max}$ can be found analytically in certain cases (see Goltermann, 1985), but in general requires an iterative calculation. The local and global critical loads are almost equal in the example where $L/h = 26.0$, and in this case we may calculate $\lambda_{max}$ as a function of the global imperfection ($f^*_{global}$) and the local imperfection ($f^*_{local}$), where

$$f^*_{global} = \xi^*_1 f_1 \tag{2}$$

$$f^*_{local} = \xi^*_2 f_2. \tag{3}$$

Table 1. I-beam. Critical loads, amplitudes of modes, 3-index and 4-index coefficients of the beam $L = 6500 = 13.0h$

| | | | |
|---|---|---|---|
| $\lambda_c^{(1)}$ | $1.1901 \cdot 10^4$ | $f_1$ | $7.8339 \cdot 10^2$ |
| $\lambda_c^{(2)}$ | $3.3370 \cdot 10^4$ | $f_2$ | $1.5453 \cdot 10^2$ |
| $\lambda_c^{(3)}$ | $6.6869 \cdot 10^4$ | $f_3$ | $1.7191 \cdot 10^2$ |
| $a_{123}$ | $-3.2216 \cdot 10^4$ | | |
| $\lambda_p/\lambda_c$ | 1.25 | 1.00 | 0.75 |
| $a_{1111}$ | $1.2751 \cdot 10^4$ | $1.3813 \cdot 10^4$ | $1.4967 \cdot 10^4$ |
| $a_{1122}$ | $-1.2260 \cdot 10^5$ | $-8.4097 \cdot 10^4$ | $-6.3023 \cdot 10^4$ |
| $a_{1133}$ | $5.0480 \cdot 10^5$ | $-3.6758 \cdot 10^6$ | $-3.4032 \cdot 10^5$ |
| $a_{2222}$ | $1.3767 \cdot 10^5$ | $1.3782 \cdot 10^5$ | $1.3800 \cdot 10^5$ |
| $a_{2233}$ | $1.9355 \cdot 10^5$ | $1.9382 \cdot 10^5$ | $1.9425 \cdot 10^5$ |
| $a_{3333}$ | $1.9178 \cdot 10^5$ | $1.9195 \cdot 10^5$ | $1.9223 \cdot 10^5$ |

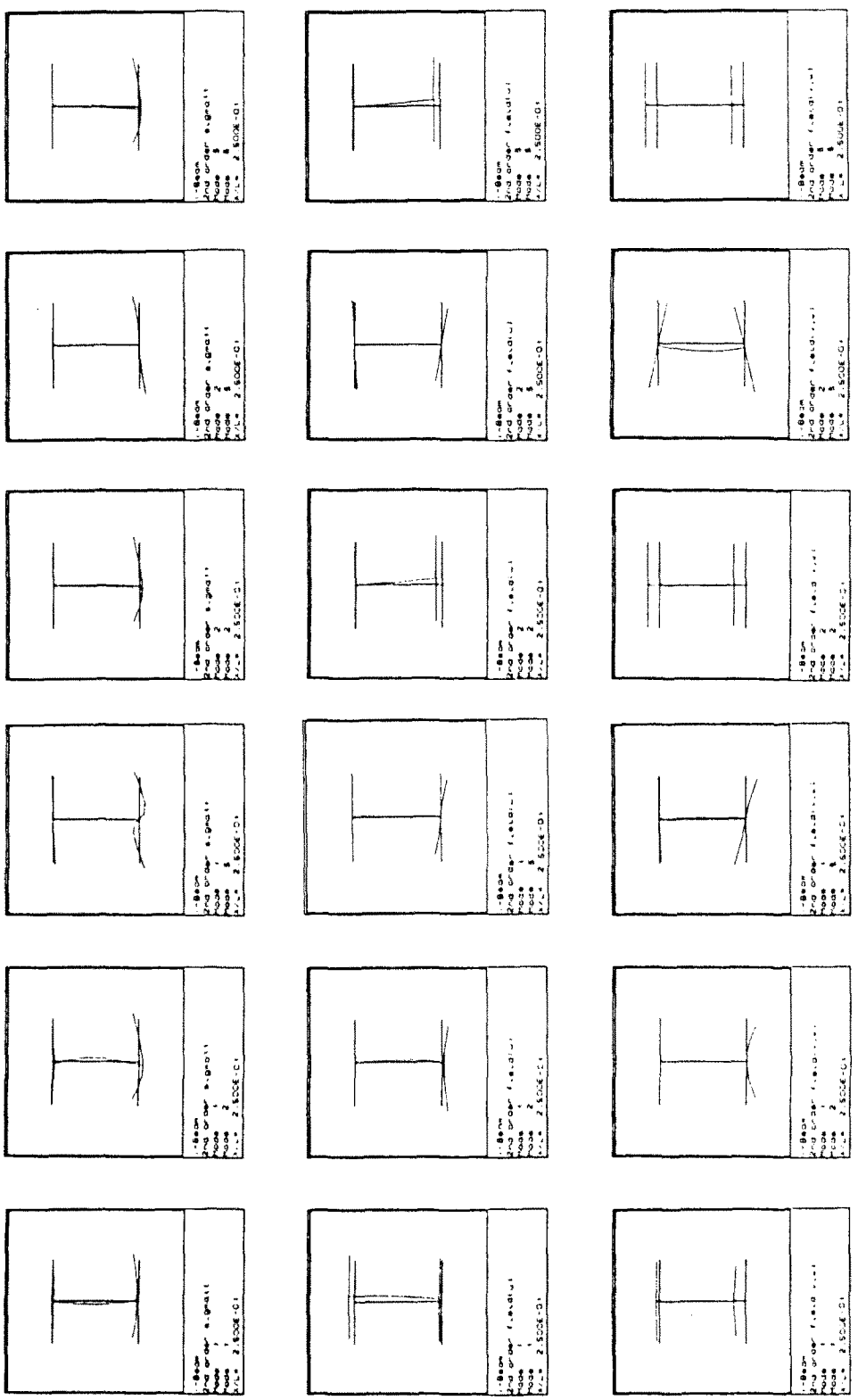

Fig. 5. The 2nd order fields at the quarter point of the beam (at $\lambda_c^{global}/\lambda_c^{local} = 3.57$ and $\lambda_p/\lambda_c = 0.75$).

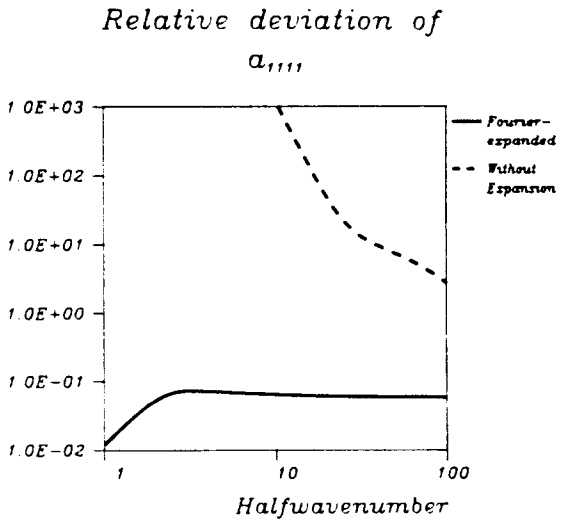


Fig. 6. Convergence of $a_{1111}$ ($L/h = 260$, $b/t = 25$).

These calculations will be based on the 1st order fields only, using a 3-mode perturbation analysis, as mentioned earlier, and giving the results shown in Fig. 8. We note a reduction of up to 60% in the load-carrying capacity due to the interaction and imperfections. [The magnitude of the imperfections corresponds to those recommended in the Danish Code of Practice on Thin-walled Structures (1984).]

We shall now include the 2nd order displacements in our calculations in order to obtain more accurate values of the load-carrying capacity than those shown in Fig. 8. We wish to examine the influence of the $\lambda$-value at which the 2nd order fields are computed ($\lambda_p$), and we therefore calculate the 2nd order fields and the 4-index coefficients for different values of $\lambda_p$ (see Table 1).

We shall also compare the results of a 2-mode analysis with those of a 3-mode analysis (including 2nd order fields in both cases). It should be noted that there will be small differences between the 2nd order fields and the 4-index coefficients computed from a 2-mode or a 3-mode analysis, respectively, due to the different orthogonality requirements in

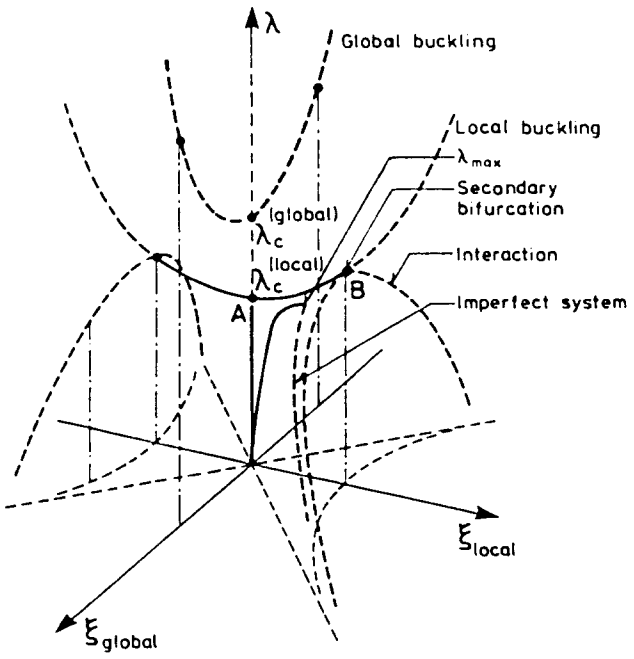


Fig. 7. Equilibrium paths.

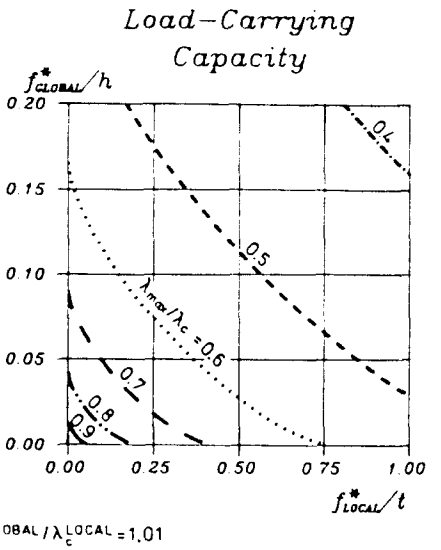


Fig. 8. $\lambda_{max}$ as a function of $f^*_{local}/t$ and $f^*_{global}/h$ at $\lambda_c^{(global)}/\lambda_c^{(local)} = 1.01$ using a 3-mode perturbation, limited to 1st order fields.

the two cases. Formulae for these differences can be obtained with the help of (32a) and (32b) in Part I, resulting in a connection between the 4-index coefficients given by

$$a_{,ijkm,\,2\text{modes}} = a_{,ijkm,\,1\text{modes}} + \frac{2(a_{,ij}\cdot a_{klm} + a_{,kl}\cdot a_{ijm} + a_{,ik}\cdot a_{jlm})}{3(\lambda_p - \lambda_c^{(1)})}. \tag{4}$$

Figure 9 shows the load-carrying capacity as a function of the local imperfection for the case of nearly equal global and local critical loads. A thin curve corresponds to a calculation based on a constant $\lambda_p$-value, but a thick curve to an interpolation between different $\lambda_p$-values determined by the condition that $\lambda_p$ should equal $\lambda_{max}$.

It can be seen from Fig. 9 that the three methods (analysis with two or three modes including 2nd order fields and $\lambda_p$-interpolation, and a 3-mode analysis based on 1st order fields only) give nearly the same results for small imperfections ($f^*_{local}/t < 0.25$), but that the deviations between the results become more pronounced with increasing imperfections. The influence of the $\lambda_p$-variation is moderate in the present case.

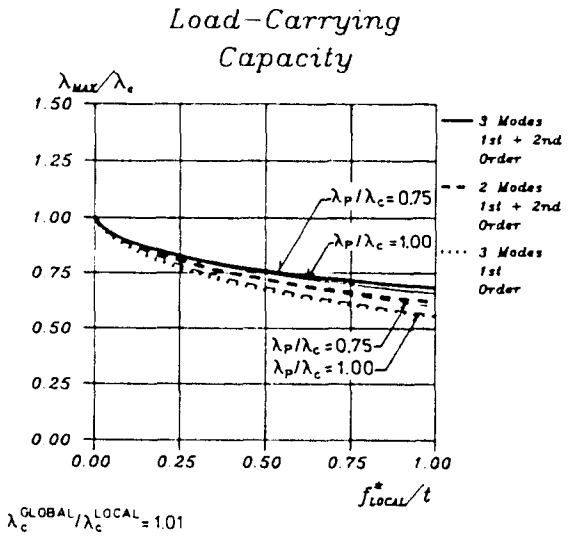


Fig. 9. $\lambda_{max}$ versus $f^*_{local}/t$ at nearly equal critical loads.

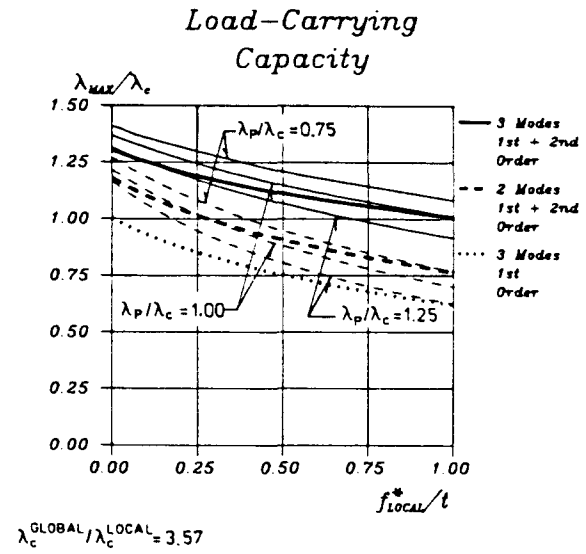


Fig. 10. $\lambda_{max}$ as a function of $f^*_{local}/t$ at $\lambda_c^{(global)}/\lambda_c^{(local)} = 3.57$.

We now repeat the calculations that lead to Fig. 9, but at a higher level of $\lambda_c^{(global)}/\lambda_c^{(local)}$ (namely 3.57), in order to examine the influence of the post-local stiffness and to investigate the possibility of reaching a load-carrying capacity above $\lambda_c^{(local)}$. Figure 10 shows the result of these calculations. It can be seen that the value of $\lambda_p$ has a significant influence on the load-carrying capacity $\lambda_{max}$, and that $\lambda_{max}$ decreases with increasing $\lambda_p$-values. We also note that the computations with 2nd order fields included predict load-carrying capacities above $\lambda_c^{(local)}$ (for small imperfections). In the previous calculations we have used the perturbation method at $\lambda$-values above $\lambda_c^{(local)}$. However, it was explained in Part I, Section 3, that the use of the perturbation method for $\lambda$-values in an interval $\lambda_a \leqslant \lambda \leqslant \lambda_b$ generally requires that all eigenfunctions with associated eigenvalues in this interval should be included among the buckling modes. In the present case we have a whole cluster of closely spaced local eigenvalues in a neighbourhood just above $\lambda_c^{(2)}$, and the associated local modes should therefore be included among the buckling modes, so that we would have to perform a multi-mode analysis. However, for the special case of purely local imperfections of the type $\xi_2^*\mathbf{u}_2$, it is shown in the Appendix that we may confine ourselves to a 3-mode analysis (with buckling modes $\mathbf{u}_1, \mathbf{u}_2, \mathbf{u}_3$) and still obtain results of a satisfactory accuracy.

We saw that $a_{123} \neq 0$, and this implies that $a_{12\Gamma} \neq 0$ when the mode $\mathbf{u}_\Gamma$ is of the same type as $\mathbf{u}_3$, and that $a_{13\Delta} \neq 0$ when the mode $\mathbf{u}_\Delta$ is of the same type as $\mathbf{u}_2$. It can now be seen from (32a) and (32b) in Part I that $\mathbf{u}_{12}$ and $a_{1122}$ will vary continuously with $\lambda$ in a neighbourhood of $\lambda_c^{(2)}$, whereas $\mathbf{u}_{13}$ and $a_{1133}$ will possess singularities for $\lambda = \lambda_c^{(\Delta)}$ (see also the values of $a_{1122}$ and $a_{1133}$ in Table 1). However, when we wish to determine the load-carrying capacity $\lambda_{max}$ for local imperfections of the type $\xi_2^*\mathbf{u}_2$, the parameter $\xi_3$ in the non-linear equations (15) in Part I will be zero, and the $\lambda_{max}$-value will not depend on $a_{1133}$. It follows that the present 3-mode analysis will not be affected by the singularities, and we obtain a valid solution by the use of the proposed method.

The behaviour of $\mathbf{u}_{12}$ and $\mathbf{u}_{13}$, and the fact that the results of a 3-mode analysis differ considerably from those of a 2-mode analysis but only slightly from an analysis with more local modes, lead us to the conclusion that the interaction is essentially an interaction of three modes, and that a 3-mode analysis should therefore be used for the present structure.

The influence of the value of $\lambda_c^{(global)}/\lambda_c^{(local)}$ on the load-carrying capacity could be described by figures such as Figs 8–10. A better and more intelligible description will be obtained by plotting $\lambda_{max}$ as a function of the ratio $\lambda_c^{(global)}/\lambda_c^{(local)}$ at certain local imperfections. This has been done using a 3-mode analysis, where we interpolate between different $\lambda_p$-values (as in Figs 9 and 10), and the results are plotted in Fig. 11. The figure shows that $\lambda_{max}$ may be greater than $\lambda_c^{(local)}$ (for small imperfections), as soon as $\lambda_c^{(global)}$ exceeds $\lambda_c^{(local)}$.

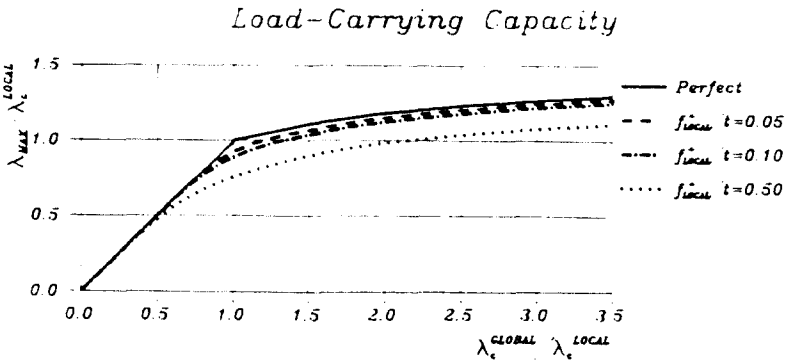


Fig. 11. The load-carrying capacity as a function of local imperfection and of $\lambda_c^{(\text{global})}/\lambda_c^{(\text{local})}$.

We also note that the imperfection-sensitivity is most pronounced when the two critical loads are nearly the same. A similar graph is presented in Fig. 5.52 of Goltermann (1985), but in that work the results are obtained by a 2-mode analysis with the 2nd order fields calculated for a constant $\lambda_p$-value. The latter graph (Fig. 5.52) shows a qualitatively similar behaviour to Fig. 11 in the present paper, although the numerical values of the load-carrying capacity differ somewhat from those of Fig. 11.

## 3. SQUARE BOX-COLUMN UNDER AXIAL COMPRESSION

The second example concerns a column with square box section as shown in Fig. 12. The column is simply supported at the ends and loaded by a compressive force $(\lambda\hat{N})$, which makes the compressive stress constant throughout the column. The value of the characteristic compressive force is

$$\hat{N} = EA \tag{5}$$

thereby making $\lambda$ equal to the compressive strain.

In the same way as in the first example we calculate the three lowest critical loads at various half wavelengths using the finite strip method, see Part I. The resulting relation between critical load $(\lambda_c)$ and half wavelength $(L_{\text{wave}})$ is plotted in Fig. 13, where one of the curves represents a double critical load. The $\lambda_c$-curve of a certain type of mode (i.e. a mode with certain symmetry properties) is always smooth, but since we show only the three lowest $\lambda_c$-values at each value of $L_{\text{wave}}$ in Fig. 13, this causes two of the curves to end rather abruptly when they cross another $\lambda_c$-curve and therefore cease to belong to the three lowest $\lambda_c$-values.

We now compare our critical loads with values obtained by means of approximate theories. For $L_{\text{wave}}/b > 10$, the global mode is rather closely approximated by the well known Euler column, as seen in Fig. 13. The local critical loads are estimated by assuming that the local modes can be represented approximately by the classical theory of plate buckling. We describe the plate deflections by the appropriate analytical solutions of plate theory, Goltermann (1985), and thereby find the critical loads by fulfilling suitable boundary conditions at the longitudinal edges. We note that the approximate critical loads provided by plate theory are quite accurate in the range $L_{\text{wave}}/b < 6$.

It can be seen that all the modes in Fig. 14 are symmetrical with respect to at least one

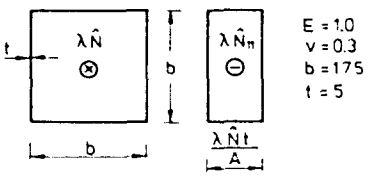


Fig. 12. Box-column geometry and load.

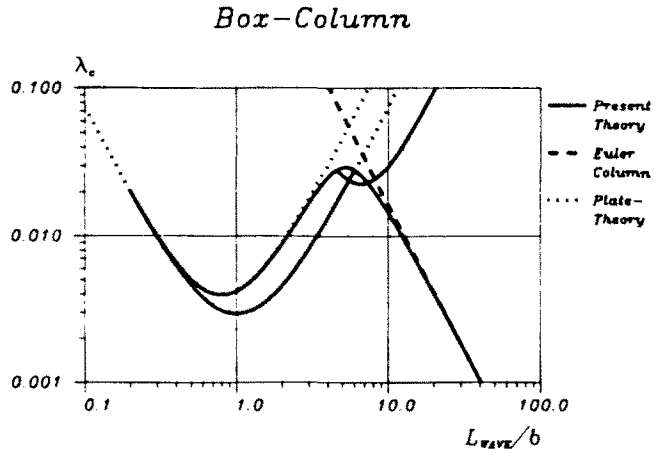


Fig. 13. Critical loads versus half wavelengths.

of the four axes of symmetry, and the present example will therefore be confined to deflections symmetrical with respect to one of those axes. The symmetry implies that it will only be necessary to perform the calculations for half the cross-section, as shown in Fig. 15.

We see in Fig. 14 that the modes satisfying the relevant symmetry conditions have the forms shown in Fig. 16, where the amplitudes are also defined. The depicted modes are the global mode $\mathbf{u}_1$ and the local modes $\mathbf{u}_2$ and $\mathbf{u}_3$, corresponding to the lowest and second lowest $\lambda_c$-curves in Fig. 13. The two local modes have the same half wavelength equal to the width of the beam ($b$), which corresponds to the local minimum on the lowest $\lambda_c$-curve. The global half wavelength is equal to the total column length ($L$) which is taken as a multiple of the width ($L/b = 14, 18, 20, 22, 24, 32$) thus giving values of $\lambda_c^{(1)}/\lambda_c^{(2)}$ equal to 2.68, 1.66, 1.36, 1.13, 0.95 and 0.54.

We use these three modes as buckling modes (1st order fields) in our interaction analysis, since the 2nd local mode $\mathbf{u}_3$ has a critical load $\lambda_c^{(3)}$ ($= 4.2021 \times 10^{-3}$) which is only 43% higher than the critical load $\lambda_c^{(2)}$ ($= 2.9446 \times 10^{-3}$) of the first local mode $\mathbf{u}_2$. We calculate the 3-index coefficients $a_{,ijk}$ by means of the finite strip method (see Part I, Section 4), and find that in general

$$a_{,ijk} = 0 \quad i,j,k \in \{1,2,3\} \tag{6}$$

except that

$$a_{123} \neq 0$$

just as in the previous example. The value of this coefficient is listed in Table 2 for $L/b = 14$, where we also find the corresponding critical loads and the amplitudes which satisfy the normality condition (9a) in Part I.

We note that it is possible, as in the previous example, to obtain an estimate of the imperfection-sensitivity based on the 1st order fields only, provided that we use a 3-mode analysis. Following the $I$-beam example we shall calculate the 2nd order fields $\mathbf{u}_{,ij}$ and the four-index coefficients $a_{,ijkm}$ at certain $\lambda$-values (denoted by $\lambda_p$).

We first consider the column with nearly equal local and global critical loads ($\lambda_c^{(1)}/\lambda_c^{(2)} = 0.95$) and calculate the 2nd order fields at various $\lambda_p$-values. Figure 17 shows a computer plot of the shape of the 2nd order fields in a beam cross-section at the quarter-point ($x/L = 0.25$) and for $\lambda_p = \lambda_c$.

If the local modes are determined approximately by plate theory, the corresponding in-plane displacements $u$ and $v$ of the local modes will be zero. In the literature, it is frequently assumed (see Benito and Sridharan, 1985a,b; Sridharan and Ashraf Ali, 1985; and Loughland and Rhodes, 1980) that the plate deflection $w$ of the 2nd order fields is equal to zero, thereby satisfying the orthogonality between the 1st and 2nd order fields. It can be seen that this is not satisfied by the more accurate solution in the present example.

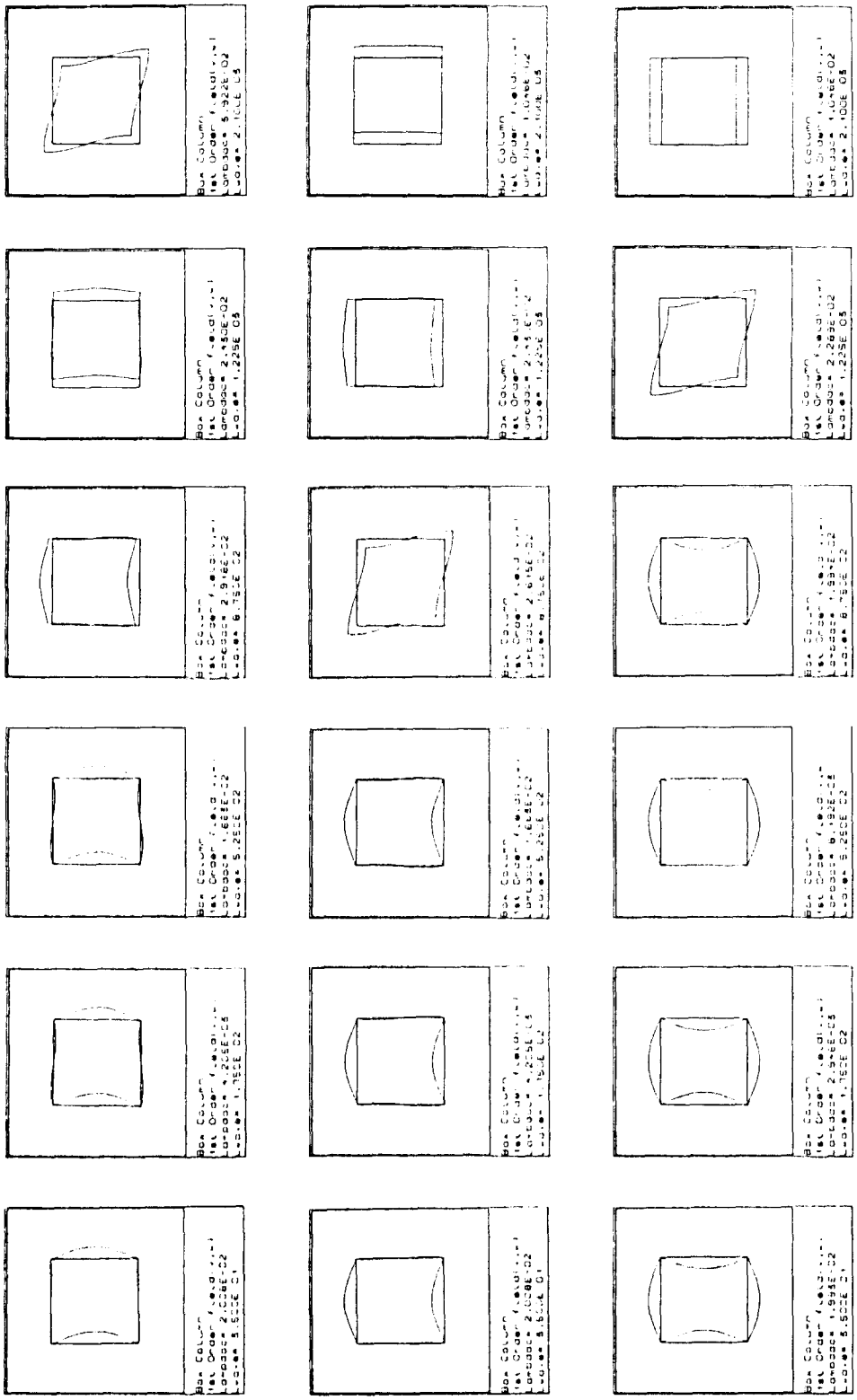

Fig. 14. Modes at different half wavelengths ($L_{x/z}$, $h = 0.2, 1, 3, 5, 7, 12$).

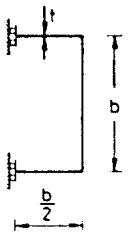


Fig. 15. Cross-section used in the analysis.

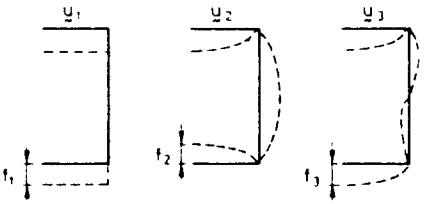


Fig. 16. Modes and amplitudes.

However, it will be a good approximation to neglect the contribution of the 2nd order $w$ to the 4-index coefficients.

Having determined the 4-index coefficients $a_{,jklm}$ (see Table 2 for $L/b = 14$), we wish to study the influence of the following factors on the load-carrying capacity of a locally imperfect column: (1) the value of the load factor $\lambda_p$ used for calculating $\mathbf{u}_{,j}$ and $a_{,jklm}$, (2) the effect of omitting the 2nd order fields and representing the displacements solely as linear combinations of buckling modes, and (3) the effect of using either a 2-mode or a 3-mode analysis (i.e. including one or two local modes, and in both cases accounting fully for the 2nd order fields).

Figure 18 shows the influence of the above three factors on the load-carrying capacity. It can be seen that the analysis with three 1st order fields (and omitting the 2nd order fields) gives a reasonably good estimate of the imperfection-sensitivity at small imperfections (just as in the case of the I-beam). When we include the 2nd order fields in our analysis, the load-carrying capacity is somewhat increased due to the post-critical stiffness of the local mode, and a small $\lambda_p$-dependence is observed. In order to investigate the possibility of attaining $\lambda_{max}$-values greater than the local critical load $\lambda_c^{(2)}$, we shall turn our attention to the shortest column, where the global critical load is significantly greater than the local critical load ($\lambda_c^{(global)}/\lambda_c^{(local)} = 2.68$).

We now wish to use the perturbation method for $\lambda$-values in a region which contains a cluster of closely spaced eigenvalues. According to the general theory of Section 3 in Part I, the associated local modes should then be included among our buckling modes. However, it is proved in the Appendix that in the case of local imperfections of the type $\xi_2^* \mathbf{u}_2$, we may restrict ourselves to a 3-mode analysis with buckling modes $\mathbf{u}_1$, $\mathbf{u}_2$, $\mathbf{u}_3$, and still obtain sufficiently accurate results.

Table 2. Box-column. Critical loads, amplitudes, 3-index and 4-index coefficients of a column with $L = 2450 = 14b$

| | | | | | | | | | | |
|---|---|---|---|---|---|---|---|---|---|---|
| $\lambda_c^{(1)}$ | $7.8840 \cdot 10^{-1}$ | | $f_1$ | $5.4004 \cdot 10^{-1}$ | | $a_{111}$ | $1.7136 \cdot 10^{-5}$ | | | |
| $\lambda_c^{(2)}$ | $2.9446 \cdot 10^{-1}$ | | $f_2$ | $5.3768 \cdot 10^{-2}$ | | | | | | |
| $\lambda_c^{(3)}$ | $4.2021 \cdot 10^{-1}$ | | $f_3$ | $7.8011 \cdot 10^{-2}$ | | | | | | |
| $\lambda_p/\lambda_c$ | 1.25 | | 1.15 | 1.00 | | 0.75 | 0.50 | | 0.25 | |
| $a_{1111}$ | $-1.1007 \cdot 10^{-8}$ | | $-1.0622 \cdot 10^{-8}$ | $-1.0604 \cdot 10^{-8}$ | | $-1.0546 \cdot 10^{-8}$ | $-1.0319 \cdot 10^{-8}$ | | $-1.0097 \cdot 10^{-8}$ | |
| $a_{1122}$ | $-1.7348 \cdot 10^{-7}$ | | $-1.0828 \cdot 10^{-7}$ | $-6.9077 \cdot 10^{-8}$ | | $-4.4577 \cdot 10^{-8}$ | $-3.3045 \cdot 10^{-8}$ | | $-2.6248 \cdot 10^{-8}$ | |
| $a_{1111}$ | $-8.3159 \cdot 10^{-9}$ | | $1.2709 \cdot 10^{-7}$ | $-1.6277 \cdot 10^{-6}$ | | $-2.0865 \cdot 10^{-7}$ | $-1.3942 \cdot 10^{-7}$ | | $-1.0943 \cdot 10^{-7}$ | |
| $a_{2222}$ | $7.8045 \cdot 10^{-8}$ | | $7.8105 \cdot 10^{-8}$ | $7.8290 \cdot 10^{-8}$ | | $7.8632 \cdot 10^{-8}$ | $7.8882 \cdot 10^{-8}$ | | $7.9125 \cdot 10^{-8}$ | |
| $a_{2233}$ | $1.5089 \cdot 10^{-7}$ | | $1.5105 \cdot 10^{-7}$ | $1.5127 \cdot 10^{-7}$ | | $1.5163 \cdot 10^{-7}$ | $1.5192 \cdot 10^{-7}$ | | $1.5221 \cdot 10^{-7}$ | |
| $a_{3333}$ | $2.9264 \cdot 10^{-7}$ | | $2.9298 \cdot 10^{-7}$ | $2.9227 \cdot 10^{-7}$ | | $2.9410 \cdot 10^{-7}$ | $2.9462 \cdot 10^{-7}$ | | $2.9505 \cdot 10^{-7}$ | |

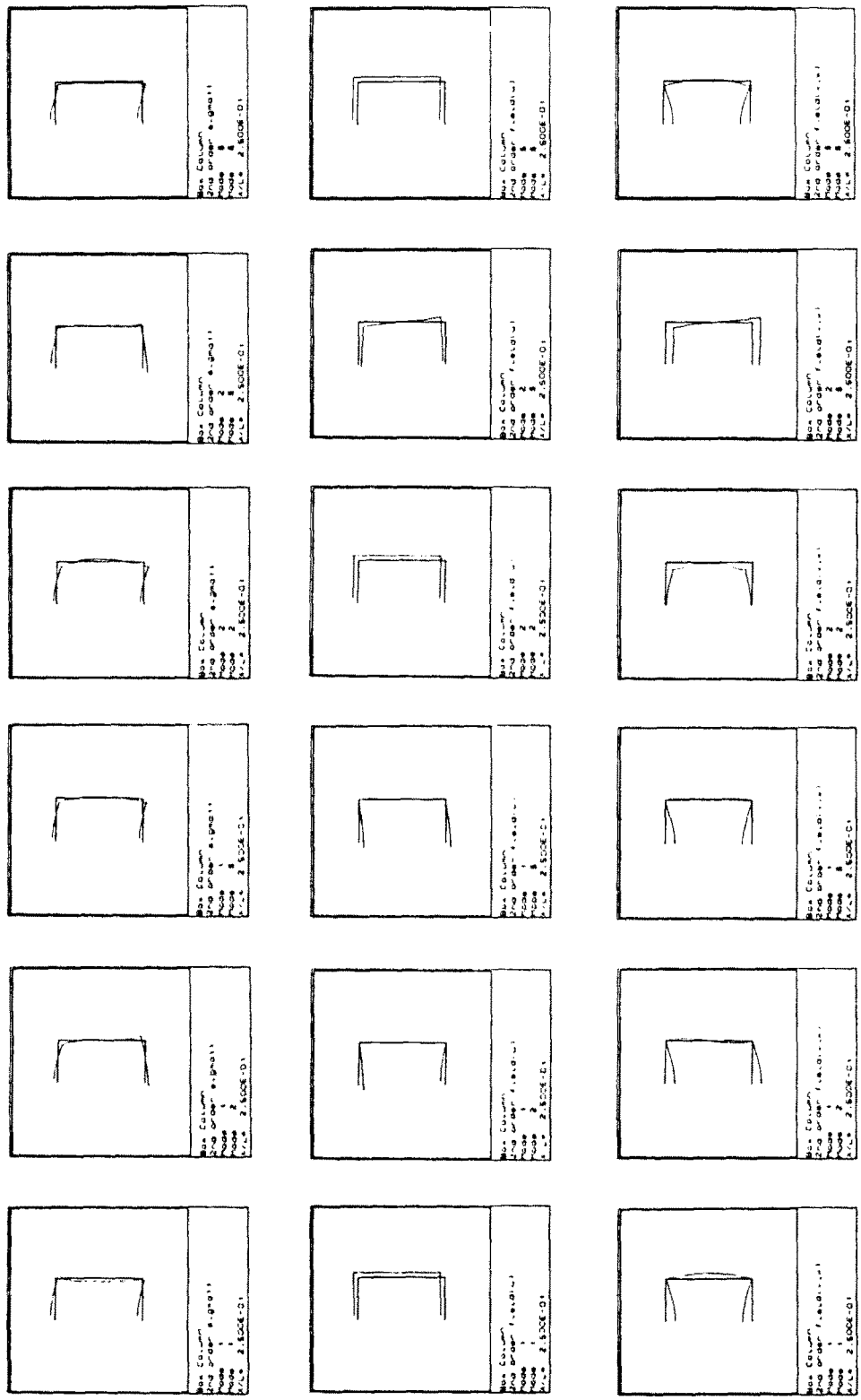

Fig. 17. Second order fields ($w/L = 0.25$, $\lambda_\rho = \lambda_c$).

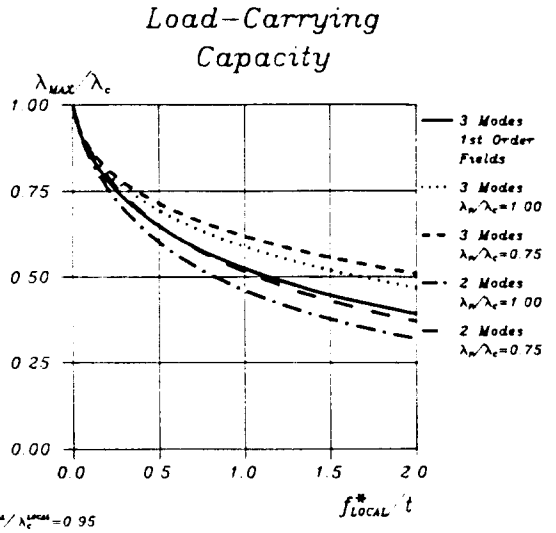


Fig. 18. Load-carrying capacity $\lambda_{max}$ versus local imperfection at nearly equal critical loads.

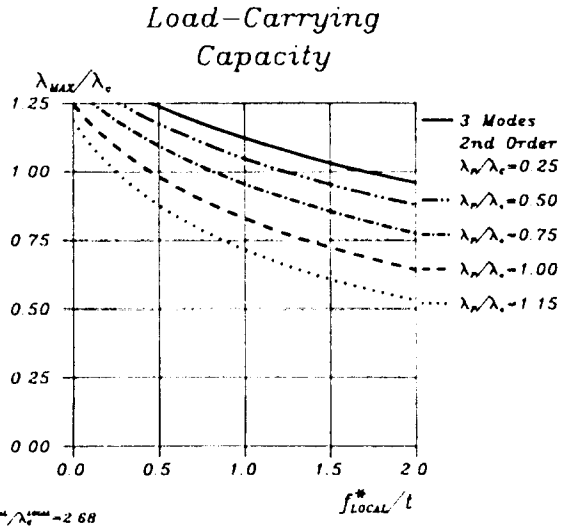


Fig. 19. Load-carrying capacity versus $\lambda_p$ and local imperfection.

The 2nd order fields and the 4-index coefficients are calculated at various $\lambda_p$-values to illustrate the influence of $\lambda_p$ (see Table 2). We compute the $\lambda_{max}$-value as a function of the local imperfection and $\lambda_p$, and the results are shown in Fig. 19. It can be seen that the influence of $\lambda_p$ on $\lambda_{max}$ is rather pronounced in this case, and we note from Figs. 18 and 19 that $\lambda_{max}$ decreases with increasing $\lambda_p$ (as long as $\lambda_p \leqslant \lambda_c^{(3)}$). A similar result is seen in the I-beam example and in Benito and Sridharan (1985a), which concerns an I-column. However, our findings differ from those of Sridharan and Ashraf Ali (1986), where there is no $\lambda_p$ dependence due to the omission of the 2nd order fields $\mathbf{u}_{12}$ and $\mathbf{u}_{13}$. These authors argue that the shape of $\mathbf{u}_{12}$ in the cross-section will be similar to that of $\mathbf{u}_3$, and that $\mathbf{u}_{12}$ will therefore be very small due to the orthogonality conditions, but this is doubtful in view of formula (32a, b) in Part I (see also the values in Table 3). In order to obtain the correct

Table 3. Box-column. Amplitudes of 2nd order fields ($L/h = 14$, $\lambda_p/\lambda_c = 1.00$, $x/L = 0.25$)

| $(i, j)$ | (1, 1) | (1, 2) | (1, 3) | (2, 2) | (2, 3) | (3, 3) |
|---|---|---|---|---|---|---|
| Sigma 11 | $3.0731 \cdot 10^{-9}$ | $1.4441 \cdot 10^{-8}$ | $2.3170 \cdot 10^{-8}$ | $1.0119 \cdot 10^{-7}$ | $2.4600 \cdot 10^{-7}$ | $3.1303 \cdot 10^{-7}$ |
| $u$ | $1.9375 \cdot 10^{-5}$ | $1.0067 \cdot 10^{-5}$ | $1.3621 \cdot 10^{-5}$ | $4.6413 \cdot 10^{-5}$ | $4.5556 \cdot 10^{-6}$ | $4.7020 \cdot 10^{-5}$ |
| $(v, w)$ | $7.0507 \cdot 10^{-5}$ | $7.1638 \cdot 10^{-5}$ | $5.0448 \cdot 10^{-4}$ | $2.0239 \cdot 10^{-6}$ | $2.5042 \cdot 10^{-5}$ | $4.5996 \cdot 10^{-5}$ |

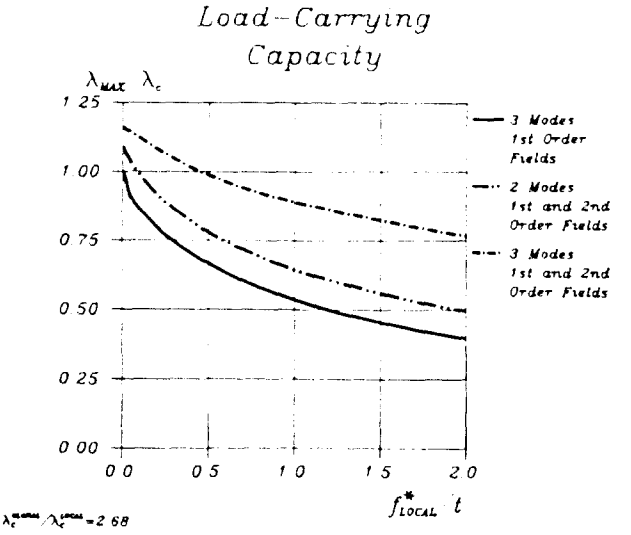


Fig. 20. Load-carrying capacity versus local imperfection.

value of $\lambda_{max}$, we must evidently put $\lambda_p = \lambda_{max}$, and we therefore interpolate between the different curves in Fig. 19 so as to get one resulting $\lambda_{max}$-curve, as shown in Fig. 20. We construct the same curves and make similar interpolations for an analysis with two modes, and also plot the resulting curve in Fig. 20.

We note that $\lambda_{max}$ may exceed the local critical load by up to 15% if we use a 3-mode analysis with 2nd order fields included, where the 2nd order fields are obviously necessary in order to account for the post-critical stiffness. Figures 18 and 20 show that a calculation with both 1st and 2nd order fields leads to higher $\lambda_{max}$-values when we use a 3-mode analysis than when we use a 2-mode analysis (as in Sridharan and Ashraf Ali, 1986). This may seem surprising in view of the fact that we have one degree of freedom less in the latter case and therefore might expect a stiffer structure. However, a 3-mode analysis must describe the behaviour more accurately than a 2-mode analysis and thus provide more accurate values of the load-carrying capacity. It is shown in the Appendix that the inclusion of additional nearly simultaneous local buckling modes in the analysis only gives rise to negligible changes in the results.

Finally, we shall determine $\lambda_{max}$ as a function of the ratio $\lambda_c^{(global)}/\lambda_c^{(local)} (= \lambda_c^{(1)}/\lambda_c^{(2)})$ and the local imperfection. In order to do this we perform the same kind of calculations and interpolations for the remaining column lengths as we did in connection with Fig. 20. The results are shown in Fig. 21. This graph shows that the load-carrying capacity may exceed the local critical load when the global critical load is greater than the local, and that the imperfection-sensitivity is most pronounced when the two critical loads are nearly equal. We observe the resemblance between the present results and the analogous results for the

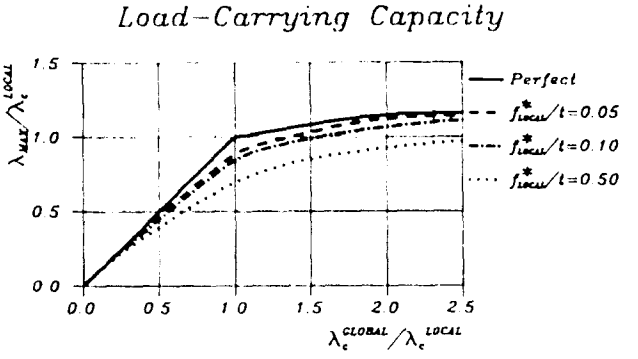


Fig. 21. Load-carrying capacity as a function of local imperfection and $\lambda_c^{(global)}/\lambda_c^{(local)}$ ratio.

I-beam (see Fig. 11). It will be seen that there is a marked difference between our results (as shown in Fig. 21) and the corresponding results for the van der Neut column (see van der Neut, 1969). However, our results agree (at least in a qualitative way) with those of Graves-Smith (1969), Koiter and van der Neut (1980), Sridharan and Benito (1984), and Sridharan and Ashraf Ali (1986), the latter concerning an I-column.

## 4. CONCLUSIONS

The post-buckling behaviour of two types of thin-walled beam structures has been investigated (lateral buckling of an I-beam, and flexural column buckling of a square box beam). The method of analysis used for these structures was presented in Part I of the authors' paper and involves a combination of the finite strip method and Koiter's asymptotic theory of stability.

It appears from both examples that substantial reductions of the load-carrying capacity (up to about 50%) occur as a result of imperfection sensitivity and mode interaction, even though each mode, by itself, corresponds to a stable-symmetric bifurcation. In both examples, it is found that, in the case of a 3-mode analysis, there is only one nonvanishing 3-index coefficient, namely $a_{123}$. This means that the mode interaction essentially involves three modes (one global and two local modes), and it is concluded that the calculations should in these examples be based on a 3-mode analysis with 2nd order fields included (to account for the post-critical stiffness of the local modes). This conclusion is confirmed by the fact that significant differences are observed in both examples between the results of a 2-mode and a 3-mode analysis.

The fact that $a_{123} \neq 0$ also means that the mixed 2nd order fields corresponding to a combination of the global and one of the local modes depend significantly on the value of the load factor at which they are evaluated ($\lambda_p$), and this implies that some of the associated 4-index coefficients will exhibit a similar $\lambda_p$-dependence. When calculating the load-carrying capacity $\lambda_{max}$, it is therefore important that the said 2nd order fields and 4-index coefficients should be evaluated at the correct value of the load factor, namely for $\lambda_p = \lambda_{max}$.

For both examples, the load-carrying capacities have been determined for different values of the ratio of global to local critical load. It is found that the load-carrying capacity may in certain cases exceed the smallest critical load. This happens if the smallest critical load corresponds to local buckling and the imperfections are local and sufficiently small. It is shown that a 3-mode analysis will be sufficiently accurate also in such cases, so that additional nearly simultaneous local buckling modes need not be included in the analysis.

## REFERENCES


Benito, R. and Sridharan, S. (1985a). Interactive buckling analysis with finite strips. *Int. J. Numer. Meth. Engng* **21**, 145–161.

Benito, R. and Sridharan, S. (1985b). Mode interaction in thin-walled structural members. *J. Struct. Mech.* **12**, 517–542.

Byskov, E. (1988). Elastic buckling problems with infinitely many local modes. *Mechanics of Structures and Machines* **15**, 413–435.

Danish code of practice on thin-walled structures, NP-152-N (1984).

Goltermann, P. (1985). Interaction between local and global stability in thin-walled beams (in Danish). Dept. of Struct. Engng, Tech. Univ. of Denmark, report No. 207.

Graves-Smith, T. R. (1969). The ultimate strength of locally buckled columns of arbitrary length. In *Thin-walled Steel Structures* (Edited by K. C. Rockey and H. V. Hill), pp. 35–60. Crosby Lockwood & Son, London.

Koiter, W. T. and Neut, A. van der (1980). Interaction between local and overall buckling of stiffened compression members. In *Thin-walled Structures* (Edited by J. Rhodes and A. C. Walker), pp. 61–82. Granada, St. Albans.

Loughland, J. and Rhodes, J. (1980). The interactive buckling of lipped channel columns under concentric or eccentric loading. In *Thin-walled Structures* (Edited by J. Rhodes and A. C. Walker), pp. 40–49. Granada, St. Albans.

Mollmann, H. (1982). Finite displacements of thin-walled beams, Parts 1 and 2. Danish Center for Appl. Math. and Mech., Tech. Univ. of Denmark, reports Nos. 252 and 253.

Mollmann, H. and Goltermann, P. (1989). Interactive buckling in thin-walled beams—I. Theory. *Int. J. Solids Structures* **25**, 715–728.

Neut, A. van der (1969). The interaction of local buckling and column failure of thin-walled compression members. In *Proc. 12th Int. Congr. Appl. Mech.* (Edited by M. Hetenyi and W. G. Vincenti), pp. 389–399. Springer, Berlin.

Pedersen, C. (1982). Stability properties and non-linear behaviour of thin-walled elastic beams of open cross-section, Parts 1 and 2. Dept. of Struct. Engng, Tech. Univ. of Denmark, reports Nos. 149 and 150.
Sridharan, S. and Ashraf Ali, M. (1985). Interactive buckling in thin-walled beam-columns. *J. Engng Mech. Div. ASCE* **111**, 1470–1486.
Sridharan, S. and Ashraf Ali, M. (1986). An improved interactive buckling analysis of thin-walled columns having doubly symmetric sections. *Int. J. Solids Structures* **22**, 429–443.
Sridharan, S. and Benito, R. (1984). Columns: static and dynamic interactive buckling. *J. Engng Mech.* **110**, 45–65.

## APPENDIX

We wish to compare the results of a 3-mode analysis (buckling modes $\mathbf{u}_1$, $\mathbf{u}_2$, and $\mathbf{u}_3$) with those of a multi-mode analysis, in which additional local modes $\mathbf{u}_\alpha$ (of the same type as $\mathbf{u}_2$) are included among the buckling modes.

In the present Appendix, small Latin indices assume the values 1, 2, 3, and small Greek indices are used to number the additional buckling modes $\mathbf{u}_\alpha$. We shall use barred symbols to denote quantities associated with the 3-mode analysis (e.g. $\bar{\mathbf{u}}_{ij}$, $\bar{a}_{ijkl}$, etc.), and unbarred symbols to denote quantities associated with the multi-mode analysis (e.g. $\mathbf{u}_{ij}$, $\mathbf{u}_{i\alpha}$, $a_{ijkl}$, $a_{ij\alpha\beta}$, etc.). We have already established some general properties of the coefficients in the equilibrium equations (see Section 4 in Part I), namely, that a 3-index coefficient vanishes when the sum of the associated wave numbers is even, and a 4-index coefficient vanishes when the sum of the wave numbers is uneven.

*Square box column*

We first consider the box column. In order to simplify the following argument, we shall introduce certain approximations. We assume that the local buckling modes $\mathbf{u}_2$, $\mathbf{u}_\alpha$, and $\mathbf{u}_3$ can be described with sufficient accuracy by conventional plate theory (this is known to be a rather good approximation). This implies that the tangential displacements $u, v$ of the local modes as well as the associated in-plane internal forces vanish, and that the normal displacement $w$ vanishes at longitudinal junctions between plate segments. The 3-index coefficients are given by (28) and (27) in Part I. Since the modes $\mathbf{u}_i$ remain unchanged when we pass from the 3-mode analysis to the multi-mode analysis, it follows that

$$a_{ijk} = \bar{a}_{ijk}. \tag{A1}$$

We proceed to consider the additional 3-index coefficients (such as $a_{ij\alpha}$, $a_{i\alpha\beta}$) that appear in the multi-mode analysis. Using the symmetry properties of the modes, and the fact that the in-plane internal forces of the local modes vanish, we find from (28) and (27) in Part I that only the 3-index coefficients

$$a_{122} \quad \text{and} \quad a_{11\alpha} \tag{A2}$$

should be taken into account in the multi-mode analysis, while the remaining 3-index coefficients are very small and can be neglected.

*4-index coefficients* – suppose that we reverse the orientation of the coordinate axes in the cross-section (the $yz$-system becomes the $y^*z^*$-system, see Fig. A1). It will be seen that, in the case of buckling modes $\mathbf{u}_2$ and $\mathbf{u}_\alpha$, the expressions for the displacements in the $y^*z^*$-system will be identical to those in the $yz$-system, while a change of sign occurs for the displacements of buckling modes $\mathbf{u}_1$ and $\mathbf{u}_3$ when we change coordinate system. This implies that a 3- or 4-index coefficient vanishes if the total number of appearances of the indices 1 and 3 is an odd number. In particular, we have

$$\left.\begin{aligned} a_{1222} = a_{122\alpha} = a_{12\alpha\beta} = a_{1\alpha\beta} = 0 \\ a_{3222} = a_{322\alpha} = a_{32\alpha\beta} = a_{3\alpha\beta} = 0 \end{aligned}\right\}. \tag{A3}$$

Now the 2nd order displacements $\mathbf{u}_{ij}$ of the multi-mode analysis are orthogonal to the additional buckling modes $\mathbf{u}_{i\alpha}$, but this will not necessarily be the case for the 2nd order displacements $\bar{\mathbf{u}}_{ij}$ of the 3-mode analysis. Using (32a) in Part I, we deduce the following relation between the two kinds of 2nd order displacements:

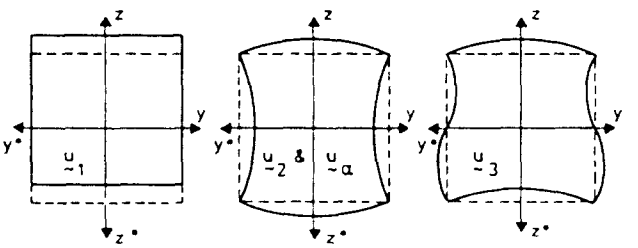


Fig. A1. Buckling modes and coordinate systems $(y, z)$ and $(y^*, z^*)$.

$$\bar{\mathbf{u}}_{ij} = \mathbf{u}_{ij} + \sum_{s} \frac{a_{ijs}}{(\lambda - \lambda_s)} \mathbf{u}_s \tag{A4}$$

where the summation is with respect to the additional buckling modes. If we now utilize the previous results concerning the 3-index coefficients [see (A2)], we conclude that

$$\mathbf{u}_{ij} = \bar{\mathbf{u}}_{ij}, \quad \text{in general, except that } \mathbf{u}_{13} \neq \bar{\mathbf{u}}_{13}. \tag{A5}$$

Inserting these results in the formulae for the 4-index coefficients [(29a) and (29b) in Part 1], we derive the following results:

$$\left.\begin{aligned} a_{1111} &= \bar{a}_{1111}, \quad a_{2222} = \bar{a}_{2222}, \quad a_{3333} = \bar{a}_{3333} \\ a_{1122} &= \bar{a}_{1122}, \quad a_{2233} = \bar{a}_{2233}, \quad a_{1133} \neq \bar{a}_{1133} \end{aligned}\right\} \tag{A6}$$

while the remaining coefficients of type $a_{ijkl}$ vanish. We proceed to study those 4-index coefficients that depend on the additional buckling modes $\mathbf{u}_s$ (such as $a_{ijks}$, $a_{ijs\beta}$, etc.). However, we shall confine our attention to the coefficients $a_{1222s}$, $a_{2222s}$, $a_{1122s}$, and $a_{2233\beta}$ since only these will be needed in the following discussion. In order to evaluate the above coefficients, we shall introduce further approximations with regard to the 2nd order displacements.

The local 2nd order fields $\mathbf{u}_{22}$, $\mathbf{u}_{2s}$, and $\mathbf{u}_{s\beta}$ will be described by von Karman plate theory. In this theory, the non-linear terms in the tangential displacements are neglected in the strain measures $\varepsilon_{s\beta}$, and this approximation will be sufficiently accurate for the present case of local buckling due to column loading, where no overall in-plane displacements of the plate segments occur. Each side of the box column is treated as a rectangular plate with the following boundary conditions: Hemp's conditions at the longitudinal junctions, and the Marguerre–Trefftz conditions at the end sections.

The in-plane forces of the approximate local 2nd order fields can now be represented by means of Airy stress functions of the form

$$\begin{aligned} &\text{for } \mathbf{u}_{22}: \psi^{(22)} = f_1(y) + g_1(y) \cos \frac{2\pi n}{l} x \\ &\text{for } \mathbf{u}_{2s}: \psi^{(2s)} = f_2(y) \cos \frac{\pi}{l} p x + g_2(y) \cos \frac{\pi}{l} (2n+p) x \\ &\text{for } \mathbf{u}_{s\beta}: \psi^{(s\beta)} = f_3(y) \cos \frac{\pi}{l} (p-q) x - g_3(y) \cos \frac{\pi}{l} (2n+p+q) x \end{aligned} \tag{A7}$$

where the wave numbers of modes $\mathbf{u}_2$, $\mathbf{u}_s$, and $\mathbf{u}_\beta$ are denoted by $n$, $(n+p)$, and $(n+q)$, respectively. It can also be shown that our approximate 2nd order fields (A7) satisfy the relevant orthogonality conditions.

It should be noted that the boundary conditions at the end sections of the approximate 2nd order fields (A7) differ from those used in our previous analysis [see (3) in Part 1]. However, for short-wave local buckling the difference in results will only be noticeable within a short distance from the end sections.

If we transform the formulae (29a) in Part 1 for the 4-index coefficients by means of Green's theorem and neglect the contribution from the 2nd order normal displacement (which can be shown to be insignificant), we find that the 4-index coefficients associated with the local modes can be expressed solely in terms of the stress functions. Using the stress functions (A7), we obtain the following results:

Let $0 < |p| < n-1$, and $0 < |q| < n-1$. Then we have

$$\left.\begin{aligned} a_{222s} &= 0 \\ a_{22s\beta} &= 0 \quad \text{for} \quad |p| \neq |q| \\ a_{22s\beta} &\neq 0 \quad \text{for} \quad |p| = |q| \end{aligned}\right\}. \tag{A8}$$

We shall not exhibit the rather long and complicated formulae which are found for the non-zero 4-index coefficients. However, Table 1A shows a comparison between the values of the 4-index coefficients provided by the present approximate method, and those obtained from a finite strip computer analysis as described in the main paper.

Table 1A.

| Coefficient | Approx. method | Finite strip computer analysis |
|---|---|---|
| $a_{2222}$ | $8.03 \cdot 10^{-8}$ | $7.81 \cdot 10^{-8}$ |
| $a_{2244}$ | $5.25 \cdot 10^{-8}$ | $5.09 \cdot 10^{-8}$ |
| $a_{2255}$ | $2.70 \cdot 10^{-8}$ | $2.62 \cdot 10^{-8}$ |
| $a_{2255}$ | $5.53 \cdot 10^{-8}$ | $5.36 \cdot 10^{-8}$ |
| $a_{4444}$ | $7.67 \cdot 10^{-8}$ | $7.44 \cdot 10^{-8}$ |
| $a_{5555}$ | $8.50 \cdot 10^{-8}$ | $8.23 \cdot 10^{-8}$ |
| Mode | $\mathbf{u}_2$ $\mathbf{u}_s = \mathbf{u}_4$ | $\mathbf{u}_\beta = \mathbf{u}_5$ |
| Wave No. | 14 15 | 13 |

| | $\xi_1$ | $\xi_3$ | $\xi_\eta$ | $\xi_\zeta$ | $\xi_\delta$ | $\xi_2$ | $\xi_\alpha$ | $\xi_\beta$ | $\xi_\gamma$ |
|---|---|---|---|---|---|---|---|---|---|
| $\xi_1$ | $\lambda_1-\lambda+3a_{1122}\xi_2^2$ | $2a_{123}\xi_2$ | 0 | 0 | 0 | 0 | 0 | 0 | 0 |
| $\xi_3$ | $2a_{123}\xi_2$ | $\lambda_3-\lambda+3a_{2233}\xi_2^2$ | 0 | 0 | 0 | 0 | 0 | 0 | 0 |
| $\xi_\eta$ | 0 | 0 | $\lambda_\eta-\lambda+3a_{22\eta\eta}\xi_2^2$ | 0 | 0 | 0 | 0 | 0 | $3a_{22\gamma\eta}\xi_2^2$ |
| $\xi_\zeta$ | 0 | 0 | 0 | $\lambda_\zeta-\lambda+3a_{22\zeta\zeta}\xi_2^2$ | 0 | 0 | 0 | $3a_{22\beta\zeta}\xi_2^2$ | 0 |
| $\xi_\delta$ | 0 | 0 | 0 | 0 | $\lambda_\delta-\lambda+3a_{22\delta\delta}\xi_2^2$ | 0 | $3a_{22\alpha\delta}\xi_2^2$ | 0 | 0 |
| $\xi_2$ | 0 | 0 | 0 | 0 | 0 | $\lambda_2-\lambda+3a_{2222}\xi_2^2$ | 0 | 0 | 0 |
| $\xi_\alpha$ | 0 | 0 | 0 | 0 | $3a_{22\alpha\delta}\xi_2^2$ | 0 | $\lambda_\alpha-\lambda+3a_{22\alpha\alpha}\xi_2^2$ | 0 | 0 |
| $\xi_\beta$ | 0 | 0 | 0 | $3a_{22\beta\zeta}\xi_2^2$ | 0 | 0 | 0 | $\lambda_\beta-\lambda+3a_{22\beta\beta}\xi_2^2$ | 0 |
| $\xi_\gamma$ | 0 | 0 | $3a_{22\gamma\eta}\xi_2^2$ | 0 | 0 | 0 | 0 | 0 | $\lambda_\gamma-\lambda+3a_{22\gamma\gamma}\xi_2^2$ |

Fig. A2. Matrix of linearized equilibrium equations for a 9-mode analysis.

It is also found from the computer analysis that all the coefficients for which the approximate analysis predicts the value zero do in fact become negligibly small.

*Equilibrium equations of multi-mode analysis*

We shall now consider the equilibrium equations of the multi-mode analysis for the case of local imperfections of the type $\xi_2^0\mathbf{u}_2$. Now, as a result of the approximate analysis described on the previous pages, we have obtained the following results [see (A2), (A3), and (A8)]:

$$a_{122} = a_{322} = 0, \quad a_{1222} = a_{3222} = 0, \quad a_{\gamma 222} = 0. \tag{A9}$$

A comparison with the nonlinear equilibrium equations (15) in Part I now reveals that a 1-mode analysis with $\xi_2 \neq 0$, $\xi_1 = \xi_3 = \xi_\gamma = 0$ will describe a possible equilibrium path. This initial equilibrium path is therefore determined by the equation

$$(\lambda_2 - \lambda)\xi_2 + a_{2222}\xi_2^3 = \lambda\xi_2^0. \tag{A10}$$

Since $a_{2222} > 0$ for the box column, the natural branch of (A10) is a constantly rising curve, and we wish to determine any branching points that may exist on this path. The condition for a branching point is that the determinant of the linearized version of the equilibrium equations (15) in Part I should vanish [the resulting equation must then be solved together with (A10)]. Using the previous results (A2), (A3), and (A8) for the coefficients we find that the determinant assumes the form shown in Fig. A2 (a determinant of a somewhat similar type was obtained by Byskov in connection with the van der Neut column; see Byskov, 1988). It will be seen that the determinant in Fig. A2 equals the product of the two determinants surrounded by dotted lines.

Consider first the small $2 \times 2$ determinant. It follows from (A1) and (A6) that the coefficients $a_{1211}$, $a_{1122}$, and $a_{2211}$ which appear in this determinant are the same for the 3-mode and the multi-mode analysis, so that the corresponding branching points will be identical for the two types of analysis.

Consider next the second (large) determinant enclosed in dotted lines. Using the values of the coefficients furnished by our approximate analysis, we can show that this determinant cannot vanish for values of $(\xi_2, \lambda)$ on the initial equilibrium path.

We conclude that, in case of the box column, we obtain the same branching points whether we use a 3-mode analysis or a multi-mode analysis (or at least very nearly the same branching points in view of the approximations that have been introduced in our multi-mode analysis).

This result was confirmed by a 5-mode computer analysis of the box column with imperfections $\xi_2^0\mathbf{u}_2$, which yielded very nearly the same results as the 3-mode analysis.

*Bending of I-beam*

In the case of the I-beam subjected to bending moments, it will not be sufficiently accurate to use von Karman plate theory to describe the local 2nd order fields, because some of these fields contain significant in-plane

displacements (see e.g. $\mathbf{u}_{22}$ in Fig. 5). It would seem, therefore, that we cannot derive reasonably simple approximate expressions for the 4-index coefficients in the present case.

However, we have performed two computer analyses of the I-beam with local imperfections $\xi\hat{\mathbf{u}}_2$ (a 5-mode and a 7-mode analysis, respectively, for the case of $L/h = 13$, $\lambda_p/\lambda_c = 1.25$, and with halfwave numbers for the modes equal to 1, 10, 10, 6, 9, 11 and 12). In both cases the corresponding branching points differ only slightly from those predicted by a 3-mode analysis. This suggests that a 3-mode analysis will be sufficiently accurate also in the case of bending of an I-beam.